THE STRUCTURE OF RADIATIVE SLOW-MODE SHOCKS

P. XU and T. G. FORBES

Institute for the Study of Earth, Oceans, and Space,
University of New Hampshire, Durham, NH 03824, U.S.A.

(Received 12 September, 1991)

Abstract. We investigate the structure of slow-mode MHD shocks in a plasma where both radiation and thermal conduction are important. In such a plasma a slow shock dissociates into an extended foreshock, an isothermal subshock, and a downstream radiative cooling region. Our analysis, which is both numerical and analytical, focuses on the nearly switch-off shocks which are generated by magnetic reconnection in a strong magnetic field. These shocks convert magnetic energy into kinetic energy and heat, and we find that for typical flare conditions about $\frac{2}{3}$ of the conversion occurs in the subshock while the remaining $\frac{1}{3}$ occurs in the foreshock. We also find that no stable, steady-state solutions exist for radiative slow shocks unless the temperature in the radiative region downstream of the subshock falls below 10^5 K. These results suggest that about $\frac{2}{3}$ of the magnetic energy released in flare loops is released at the top of the loop, while the remaining $\frac{1}{3}$ is released in the legs of the loop.

1. Introduction

It has long been recognized that magnetic reconnection plays a very important role in solar flare phenomena (Giovanelli, 1947; Sweet, 1958; Parker, 1963; Petschek, 1964; Sonnerup, 1979, 1984; Priest, 1984, 1985), and magnetic reconnection has been used to explain the observed energy release in solar flares and the formation of the flare loops (Parker, 1984; Malherbe, Forbes, and Priest, 1984; Forbes, 1986; Priest and Forbes, 1986; Low and Wolfson, 1988; Forbes, Malherbe, and Priest, 1989). Solar flare loops, with their temperature ranging from 10^4 to 3×10^7 K, are unusually dense compared with the surrounding corona (Lin, Lin, and Kane, 1985; Withbroe, 1978; Zirin, 1986; Heinzel and Karlický, 1987), and they are long-lived features which may persist for 10 hours or more. An enormous amount of material – greater than the mass of the entire corona – flows through the flare loops system during its lifetime (Kleczek, 1964; Kopp and Pneuman, 1976). Thus, the evolution of the flare loops involves not only reconnection, but also the additional processes of chromospheric ablation and thermal condensation (Sturrock, 1972; Hirayama, 1974; Ohki, 1975; Schmieder *et al.*, 1987; Forbes and Malherbe, 1986a, b).

MHD slow-mode shocks, which were first introduced in reconnection theory by Petschek (1964), are the key link between magnetic reconnection and chromospheric ablation (see, e.g., Cargill and Priest, 1982). To see why this is so, consider Figure 1 which shows the expected shock pattern in the reconnection model of flare loops by Forbes, Malherbe, and Priest (1989). According to this model reconnection occurs at a coronal x-line which lies at the intersection of two pairs of slow-mode shocks. These shocks convert magnetic energy into bulk flow kinetic energy and heat. Due to the strong thermal conduction along the field lines, the slow shocks dissociate into isothermal

Solar Physics **139:** 315–342, 1992.

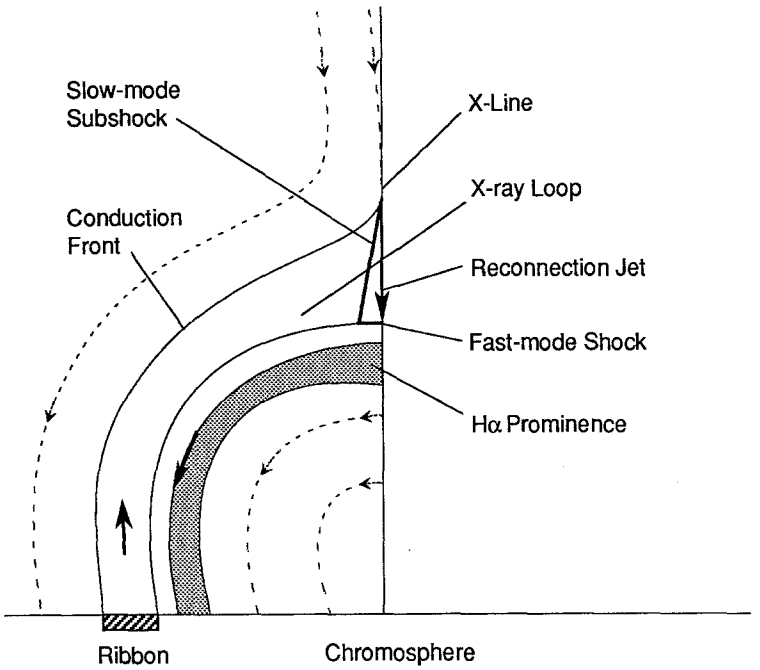

Fig. 1. Expected flow pattern in the reconnection model of flare loops. Chromospheric ablation is continually driven by heat released from magnetic field annihilation. As field lines are reconnected, the loops grow in size, and the ribbons propagate outward, away from the axis of symmetry (after Forbes, Malherbe, and Priest, 1989).

subshocks and foreshocks (thermal conduction fronts) (Forbes and Malherbe, 1986b), but the jump conditions across the total shock transition, from upstream of the foreshock to downstream of the subshock, are given by the usual slow-mode jump conditions. The foreshocks and the subshocks annihilate the magnetic field in the plasma flowing through them, and the thermal energy released in the annihilation is spread out all along the field lines. Consequently the heat is conducted from the corona to the chromosphere and leads to extensive heating and ablation of chromospheric plasma, creating and sustaining the hot X-ray loops.

The thickness of the total shock transition is of the order of the scale-size of the loops. Therefore, the total transition can no longer be considered strictly as a shock since its thickness is not small compared to its extension in the other dimensions. However, the subshocks still exist as proper shocks, although strictly speaking they should no longer be thought of as subshocks.

The plasma which crosses the subshocks forms a pair of reconnection jets which are directed towards and away from the photosphere. Unlike the upward jet, the downward jet forms on field lines which are connected to the chromosphere. Consequently, evaporation injects dense chromospheric plasma into the lower jet but not into the upper one. Because the downward jet is supermagnetosonic with respect to the fast-mode wave speed, it terminated at a fast shock (termination shock) below which is region of

deflected flow, forming a deflection sheath (see Forbes, 1986). As reconnection proceeds, the x-line moves upward, and field lines on which the ablated plasma is flowing move through the termination shock and become disconnected from the subshocks. Once the field lines are disconnected, the plasma on them is no longer heated, and it immediately begins to cool. During the cooling, a thermal instability is triggered and the plasma temperature drops below the corona temperature. This cool plasma forms the visible Hα loop prominence where the cool plasma flows, or falls, down the legs of the loops and returns to the chromosphere.

In the past 25 years, studies of the structure, the stability, and the propagation of slow-mode shocks in different aspects (Kantrowitz and Petschek, 1966; Coroniti, 1970; Bel and L.-Micoulant, 1973; Rosenau and Frankenthal, 1978; Swift, 1983; Feldman *et al.*, 1984, 1985, 1987; Hada and Kennel, 1985; Winske, Storer, and Gary, 1985; Edmiston and Kennel, 1986; Kennel, 1987, 1988; Richter, 1988) have built up a considerable knowledge base about slow shocks. However, very little work has yet been done on the radiative slow shocks involved in the evolution of solar flares.

The structure of slow shocks becomes much more complicated when radiation and thermal conduction are both taken into consideration. The large density of the flare loops makes radiative cooling a significant factor in the energy equilibrium. The effect of radiation on shock wave behavior in fluid dynamics has long been studied. One of the first studies on radiative fluid dynamic shocks was done by Marshak (1958). And some authors have studied radiative shocks in connection with the evolution of supernova remnants (Cox and Tucker, 1969; Cox, 1972a, b; Chevalier, 1974; Chevalier and Theys, 1975). An analysis of radiative shocks must necessarily include coronal heating to reflect the radiative coupling with the surrounding coronal environment. Accordingly, when talking about radiative cooling, we consider both radiative cooling and coronal heating as a united process unless otherwise specified.

The purpose of this paper is to present a theoretical analysis on the structure of radiative slow shocks. In addition to the foreshock and the subshock there is a radiative cooling region downstream of the subshock. The plasma flowing through this region radiates the excess heat generated during its passage through the shock. Some radiative loss also occurs in the foreshock region, but in general the dominant radiative loss occurs in the downstream region.

It should be kept in mind that the very concept of a simple planar shock transition is not directly applicable to flare loops, since in flare loops the foreshock region extends all the way from the reconnection site to the chromosphere. This distance is on the order of the size of the loops, the total shock transition cannot be considered planar. The actual problem of the structure of the flare loops is more complicated than the problem of planar shocks. Furthermore, in flare loops ablation of chromospheric plasma by the conduction electrons and energetic particles is a dominant factor in the formation of the loops. Since we ignore this ablation process in this paper and assume shocks to be planar, our analysis of radiative slow-mode shocks represents only a first step in modeling the actual structure of flare loops.

For purposes of comparison and illustration we first consider the structure of radia-

tive gas dynamic shocks in a thermally conducting medium. Following this, we then determine the structure of MHD switch-off shocks where the component of magnetic field tangential to the shock is annihilated completely. Switch-off shocks are very good approximation to the type of slow shocks that are likely to exist when reconnection occurs in the corona (Petschek, 1964).

2. Basic MHD Equations

The fundamental MHD equations used here are given by Priest (1982b). We consider the stationary movement of a plane shock propagating along the positive x-direction at a speed V_0. Two coordinate systems are adopted: the laboratory frame in which the fluid upstream of the shock is at rest, while the shock wave propagates through it; and a shock-rest frame in which the shock stays at rest while the fluid flows through it at the velocity $-V_0$ as shown in Figure 2.

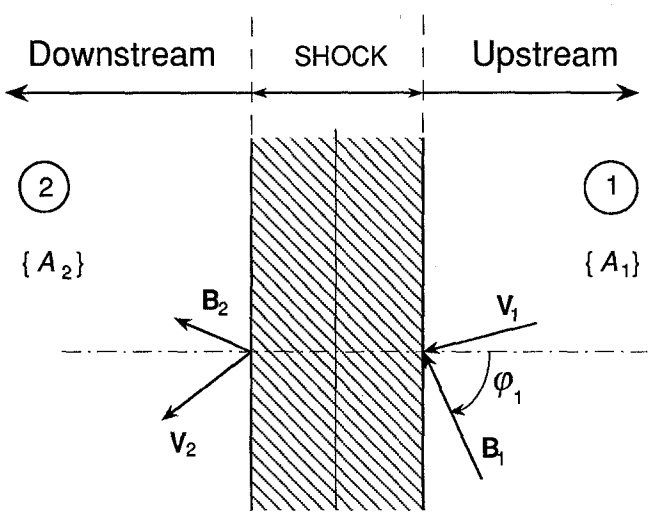

Fig. 2. Schematic diagram of slow shock geometry in shock-rest frame. The upstream and downstream parameters are labeled by subscripts 1 and 2, respectively.

The shock-rest frame is related to the laboratory frame by transformation $z = x - V_0 t$. Accordingly, in the shock-rest frame, the MHD equations are:

$$P = \rho R T , \tag{1a}$$

$$\mathrm{d}B_x/\mathrm{d}z = 0 , \tag{1b}$$

$$\mathrm{d}(\rho V_x)/\mathrm{d}z = 0 , \tag{1c}$$

$$\mathrm{d}[V_x B_y + V_y B_x + \eta(\mathrm{d}B_y/\mathrm{d}z)]/\mathrm{d}z = 0 , \tag{1d}$$

$$\mathrm{d}[P + B_y^2/2\mu + \rho V_x^2 + (4\rho\nu/3)(\mathrm{d}V_x/\mathrm{d}z)]/\mathrm{d}z = 0 , \tag{1e}$$

$$\mathrm{d}(\rho V_x V_y + B_x B_y/\mu + \rho\nu(\mathrm{d}V_y/\mathrm{d}z))/\mathrm{d}z = 0\,, \tag{1f}$$

$$\gamma P\,\mathrm{d}V_x/\mathrm{d}z + V_x\,\mathrm{d}P/\mathrm{d}z + (\gamma - 1)\{\mathrm{d}(\kappa\,\mathrm{d}T/\mathrm{d}z)/\mathrm{d}z - \rho^2 Q(T) + \rho H_c + \\ + \eta(\mathrm{d}B_y/\mathrm{d}z)^2/\mu + \rho\nu[4(\mathrm{d}V_x/\mathrm{d}z)^2/3 + (\mathrm{d}V_y/\mathrm{d}z)^2]\} = 0\,, \tag{1g}$$

where P, ρ, T, γ, R, and μ denote the pressure, the density, the temperature, the ratio of specific heats, the gas constant, and the magnetic permeability, respectively. The quantities $B_x(V_x)$ and $B_y(V_y)$ are the normal and the tangential components of magnetic field (velocity), and $V_x = V_0 - v$, where v is the perturbed fluid velocity (in the lab frame) normal to the shock. The dissipation coefficients are the magnetic diffusivity η, the kinematic viscosity ν, and the thermal conduction κ. The optically thin raditive cooling is characterized by cooling function $\rho^2 Q(T)$, while coronal heating is characterized by the heating function ρH_c, where H_c is a constant.

In an ideal fluid shock are discontinuities, since ν, η, and κ vanish. However, for a real fluid with finite dissipation coefficients, shocks are transition layers in which dissipation effects are balanced by nonlinear effects. The 'thickness' of the transition layer is measured by the scale length of the corresponding dissipation.

To emphasize the effect of radiative cooling, we treat η, ν, and κ as constants throughout our work so that we can focus on the study of radiation. We also adopt a reasonable assumption often used in solar flare research (Priest, 1982a; Forbes, Malherbe, and Priest, 1989), i.e., the scale lengths of viscosity L_ν and resistivity L_η are comparable but much smaller than thermal scale length L_κ.

Radiative cooling function $Q(T)$ takes form of $\tilde{\chi}T^\alpha$, where $\tilde{\chi}$ and α are piecewise constants (Cox and Tucker, 1969; Priest, 1982b). For simplicity we consider two simple approximations: first, a single value of α, i.e., $\alpha = 2$, $\tilde{\chi}$ is constant for all temperature; and second, two values of α, i.e., $\alpha = 2$ when $T < T_c$ and $\alpha = -\frac{1}{2}$ when $T > T_c$ with corresponding constants $\tilde{\chi}$ for each α value. The temperature T_c is defined as the critical temperature at which $Q(T)$ reaches a maximum.

The occurrence of slow shocks requires $V_0 > C_{sL1}$, where C_{sL1} is slow-made wave speed given by the smaller value of

$$C_{sL1}^2 = \tfrac{1}{2}\{C_{A1}^2 + C_{s1}^2 \pm [(C_{A1}^2 + C_{s1}^2)^2 - 4C_{A1}^2 C_{s1}^2 \cos\varphi_1]^{1/2}\}\,. \tag{2a}$$

For isothermal subshocks, the condition is $V_{xd} < \tilde{C}_{sLd}$ (Coroniti, 1970), where $\tilde{C}_{sLd}$ is the downstream isothermal slow-mode wave speed given by the smaller value of

$$\tilde{C}_{sLd}^2 = \tfrac{1}{2}\{C_{Ad}^2 + \tilde{C}_{sd}^2 \pm [(C_{Ad}^2 + \tilde{C}_{sd}^2)^2 - 4C_{Ad}^2\tilde{C}_{sd}^2\cos\varphi_d]^{1/2}\}\,, \tag{2b}$$

where C_A, C_s, $\tilde{C}_s$, and φ denote the Alfvén speed, the sound speed, the isothermal sound speed, and field direction, respectively. The upstream (downstream edge of subshock) parameters are labeled by subscript $1(d)$. Coroniti's condition indicates that an isothermal subshock occurs when the total shock strength exceeds the critical value so that the dissipation of thermal conduction can no longer balance the nonlinear effect of the strong shock, hence the additional dissipations, such as viscosity, have to be introduced.

It is usually assumed that the motion of fluid outside the total transition layer is

uniform and steady (in the shock-rest frame). Hence, $d/dz = 0$ except within the transition layer. This physical consideration requires, therefore, that radiative cooling be balanced by coronal heating outside the total transition layer. The outer boundary conditions (OBC), i.e., the equilibrium conditions, are expressed accordingly as

$$\rho^2 Q(T) - \rho H_c \to 0 \quad \text{as} \quad z \to \infty \text{ or } z \to -\infty , \tag{3a}$$

$$d/dz \to 0 \quad \text{as} \quad z \to \infty \text{ or } z \to -\infty , \tag{3b}$$

$$A \to A_1 \quad \text{as} \quad z \to \infty , \tag{3c}$$

$$A \to A_2 \quad \text{as} \quad z \to -\infty ; \tag{3d}$$

here A denotes an arbitrary physical parameter (see Figure 2).

The above OBC are often given as general BC of the MHD Rankine–Hugoniot (R–H) relations, since all the transition are confined within the total shock layer. However, this is not the case when radiative cooling in the downstream of the subshock is considered. Equation (3a) describes the equilibrium requirement in the far downstream region, which, in general, is not satisfied by MHD R–H relations. According to Kennel (1987), isothermal subshock occurs at the downstream edge of the total shock transition. Therefore, MHD jump relations specifies the parameters at downstream edge of the subshock rather than those in the far downstream region. So the region immediate downstream of the subshock is no longer uniform. Instead, an intermediate region called radiative cooling region, in which the variation of physical parameters is mainly due to the effect of radiation, occurs between the subshock and the far downstream. The total transition layer is no longer the same as the total shock layer. It now consists of the total shock layer and radiative cooling region. Thus we define the inner boundary conditions (IBC) of radiative slow shock as those MHD jump relations for the total shock as well as the subshock transition. Our IBC may also include the non-zero derivatives of the physical parameters at upstream and downstream edges of the subshocks, if necessary. Despite of the fact that the so-called inner boundary conditions actually depend on the OBC, it is necessary to distinguish between them because they have different physical meanings.

3. Gas Dynamic Shocks

The elimination of magnetic field simplifies Equations (1) to

$$P = \rho R T , \tag{4a}$$

$$d(\rho V)/dz = 0 , \tag{4b}$$

$$d[P + \rho V^2 + (4\rho\nu/3)(dV/dz)]/dz = 0 , \tag{4c}$$

$$\chi P \frac{dV}{dz} + V \frac{dP}{dz} + (\gamma - 1)\left[\frac{d}{dz}\left(\kappa \frac{dT}{dz}\right) - \rho^2 Q(T) + \rho H_c + \frac{4}{3}\rho\nu\left(\frac{dV}{dz}\right)^2\right] = 0 . \tag{4d}$$

The OBC (see Equations (3)) give

$$[\rho Q(T) - H_c]|_1 = [\rho Q(T) - H_c]|_2 . \tag{5a}$$

The IBC (derived by integrating Equations (4b)–(4d)) give

$$X = \frac{(\gamma + 1)M_1^2}{\gamma M_1^2 + 1 - \sqrt{(M_1^2 - 1)^2 + \Delta}} , \tag{5b}$$

$$Y = \frac{\gamma M_1^2 + 1 + \gamma\sqrt{(M_1^2 - 1)^2 + \Delta}}{\gamma + 1} , \tag{5c}$$

$$X_s = X\eta_g - 1 , \tag{5d}$$

where M_1 is the upstream Mach number,

$$\eta_g = (P_1 + \rho_1 V_0^2)/\rho_1 V_0^2 = 1 + 1/\gamma M_1^2 , \qquad \Delta = 2(\gamma + 1)M_1^4 I ,$$

$$I = \frac{\gamma - 1}{\rho_1 V_0^3}\left\{\left(\kappa \frac{\mathrm{d}T}{\mathrm{d}z}\right)\Big|_d - \frac{4}{3}\frac{\rho_1 V_0 \nu}{\gamma - 1}\left(\frac{\mathrm{d}V}{\mathrm{d}z}\right)\Big|_d + \int_d^1 \rho[\rho Q(T) - H_c]\,\mathrm{d}z\right\} ,$$

and $V_0 = V_1$. The quantities X and Y represent the total shock jump, and X_s gives the subshock jump:

$$X = \frac{V_1}{V_d} = \frac{\rho_d}{\rho_1} , \qquad Y = \frac{P_d}{P_1} , \qquad X_s = \frac{V_s}{V_d} = \frac{\rho_d}{\rho_s} = \frac{P_d}{P_s} .$$

Thus, Coroniti's condition becomes $X_s > 1$.

The above OBC and IBC imply that radiative cooling affects the shock structure mainly in two ways. First, as an integral effect, radiative cooling changes the jump conditions for shocks and subshocks since the ordinary jump relations are replaced by Equations (5). Second, radiative cooling creates a radiative region attached at the downstream edge of the isothermal subshock. The extent of the first effect depends on the thickness of the shock because if the shock is very thin, the radiative loss within the shock is negligible. Figure 3 shows a schematic plot of the shock geometry. The thicknesses of the shock and the subshock are determined by thermal and viscous scale lengths, respectively. Fluid flows through the various regions which are indicated as follows:

upstream of total shock transition – [1], foreshock – [F],

upstream edge of subshock – [s], downstream edge of subshock – [d],

radiative cooling region – [C], far downstream of shock – [2].

In this paper we assume that the subshock is very thin compared to all other scale lengths, or equivalently, that $\nu = 0$ (we also expect $\eta = 0$ because we assume $\nu \sim \eta$).

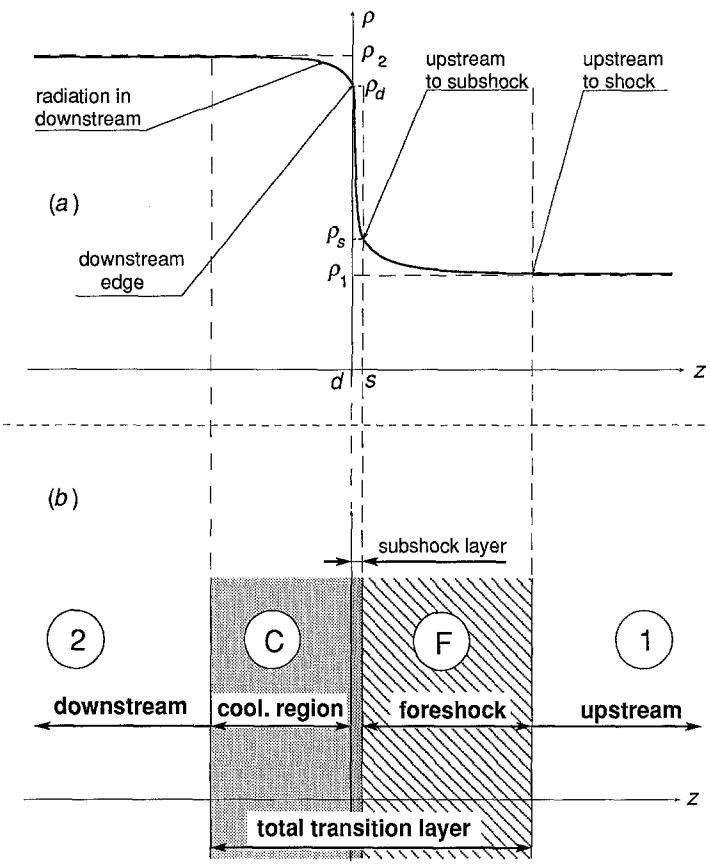

Fig. 3. Schematic diagram for hydrodynamic shock structure: (a) density curve, (b) different regions of shock structure. Subscripts d and s denote the downstream and upstream edges of subshock, respectively.

Thus the radiative energy loss within the subshock is negligible. By contrast, we assume the foreshock to be very thick, so that the radiative loss in the foreshock is not negligible.

3.1. Radiation alone

To discuss radiative cooling process we first consider the simple case in which thermal conduction is zero. The total shock transition reduces into a discontinuity when $\kappa = 0$, and the jump conditions are those of an ordinary gas dynamic shock. The solution for region C is easily found by substituting $v = 0$ and $\kappa = 0$ into (4), that is

$$V = uV_1\,, \tag{6a}$$

$$\rho = \rho_1/u\,, \tag{6b}$$

$$P = \rho_1 V_0^2/(\eta_g - u)\,, \tag{6c}$$

$$T = V_0^2(\eta_g - u)u/R\,, \tag{6d}$$

where $u(z)$ is the normalized gas velocity satisfying

$$[\gamma\eta_g - (\gamma + 1)u]\, du/dz = (\gamma - 1)\rho[\rho Q(T) - H_c]/(\rho_1 V_0^3)\,, \tag{7}$$

with $Q(T) = \tilde{\chi} T^{\alpha}$ and $d/dz \to 0$ (as $z \to -\infty$), i.e.,

$$H_c = \rho_1 Q(T_1) = \rho_2 Q(T_2)\,. \tag{8}$$

The matter we are amost concerned about is whether or not the above equations lead to a physically realistic solution. Let us first look at the case $\alpha = 2$.

Substituting $\alpha = 2$ into Equation (8) produces a cubic equation for u, namely,

$$[u(\eta_g - u)^2]|_2 = (\eta_g - 1)^2\,. \tag{9}$$

It has three roots ($u_+ > u_0 > u_-$),

$$u_0 = 1$$

and

$$u_{\pm} = [2\eta_g - 1 \pm (4\eta_g - 3)^{1/2}]/2\,.$$

The quantity u_0 represents the trivial solution of no shock at all because it gives a downstream velocity which is the same as the upstream velocity. The solution u_+ gives an unphysical solution because it leads to a negative value for the downstream pressure. Thus the only choice for a physical solution is

$$u_2 = u_- = [2\eta_g - 1 - (4\eta_g - 3)^{1/2}]/2\,. \tag{10}$$

Equation (7) can be normalized and rewritten as an autonomous system,

$$\frac{du}{d\xi_R} = \frac{\gamma - 1}{u}\,\frac{(u-1)(u-u_2)(u-u_+)}{\gamma\eta_g - (\gamma+1)u}\,, \tag{11}$$

where $\xi_R = z\rho_1 Q(T_1)/[V_0^3(\eta_g - 1)^2]$. Critical-point analysis (Bender and Orszag, 1978) shows that $u = u_2$ is a stable node of the system (11). This means that the conbined effect of radiative cooling and wave heating is to drive the system towards thermal equilibrium in the downstream region when $\alpha = 2$. This conclusion can be generalized further to all α satisfying

$$\alpha > \frac{\eta_g - u^*}{\eta_g - 2u^*} = \alpha_0\,, \tag{12}$$

where $1 < \alpha_0 < \infty$, and u^* represents the expected solution of Equation (8). For the other values of α, the effect of radiative cooling is to drive the system away from equilibrium, and thus the system is thermally unstable. In other words, the plasma flow will approach equilibrium in the downstream region only when condition (12) is satisifed, otherwise no proper equilibrium can be reached.

The cooling function $Q(T)$ in the temperature range appropriate for the corona and flare loops (10^4–3×10^7 K) may be roughly modeled as (see Priest, 1982b)

$$Q(T) = \begin{cases} Q_<(T) = \tilde{\chi}_< T^2, & T < T_c, \\ Q_>(T) = \tilde{\chi}_> T^{-1/2}, & T > T_c, \end{cases} \tag{13}$$

where $\tilde{\chi}_> = 10^{-31.5}$, $\tilde{\chi}_< = 10^{-44}$, and $T_c = 10^5$ K. The velocity u_c, corresponding to T_c, is

$$u_c = \tfrac{1}{2}[\eta_g - \sqrt{\eta_g^2 - 4T_c/(V_0^2/R)}] .$$

Since we wish to apply our results to flare loops we will assume that the upstream temperature corresponds to the temperature of the chromosphere (2×10^4 K) rather than the corona (10^6 K). Hence, in the upstream region we set $\alpha = 2$ and $H_c = \rho_1 Q(T_1) = \rho_1 \tilde{\chi}_< T_1^2$. According to the previous discussion and condition (12), the equilibrium in the downstream region is approached only when $\alpha = 2$ (i.e., $T < T_c$). Thus the cooling in region C is governed by

$$\frac{du}{d\xi_R} = \frac{\gamma - 1}{u} \frac{(u-1)(u-u_2)(u-u_+)}{\gamma\eta_g - (\gamma+1)u}, \qquad u < u_c, \tag{14a}$$

$$\frac{du}{d\xi_R} = \frac{\gamma - 1}{u[\gamma\eta_g - (\gamma+1)u]} \left[\frac{(T_c R/V_0^2)^{5/2}}{u^{3/2}(\eta_g - u)^{1/2}} - (\eta_g - 1)^2 \right], \quad u > u_c . \tag{14b}$$

3.2. Radiation and thermal conduction combined

The differential equation for the velocity u in a radiative gas dynamic shock with thermal conduction as derived from Equations (4) is

$$[\gamma\eta_g - (\gamma+1)u]\, du/d\xi = D_{RC} - dQ_g/d\xi , \tag{15}$$

where $\xi = Z/L_\kappa$, the length L_κ is the thermal scale length of the total shock defined by $L_\kappa = \gamma\kappa/(\rho_1 c_p V_0)$, and D_{RC} is the differential energy loss due to radiative cooling, i.e.,

$$D_{RC} = (\gamma - 1) R_L u_c [\rho_1 Q(T)/(uH_c) - 1]/u , \tag{16}$$

where $R_L = L_\kappa H_c/u_c V_0^3$ is a dimensionless constant representing the ratio of the thermal scale length L_κ to characteristic length of radiative cooling L_R, defined by $L_R = u_c V_0^3/H_c$.

For the two-value α case, D_{RC} is

$$D_{RC} = (\gamma - 1) R_L u_c [u(\eta_g - u)^2/T_1^2 - 1]/u , \qquad T < T_c , \tag{17a}$$

$$D_{RC} = (\gamma - 1) R_L \frac{u_c}{u} [(T_c/T_1)^2 u^{-3/2} \sqrt{T_c/(\eta_g - u)} - 1] , \quad T > T_c . \tag{17b}$$

The normalized heat flux ($\kappa\nabla T$) is

$$Q_g = d[u(\eta_g - u)]/d\xi = (\eta_g - 2u)\, du/d\xi . \tag{18}$$

The BC of Equation (15) is given by Equations (5) and $v = 0$, where Δ is replaced

by $\Delta_g = 2(\gamma + 1)M_1^4 I_g$, and

$$I_g = R_c + Q_g|_d = \int_d^1 D_{RC}\,\mathrm{d}\xi + [(\eta_g - 2u)\,\mathrm{d}u/\mathrm{d}\xi]|_d\,.$$

Do Equation (15) and its accompanying BC lead to a physical solution? The answer can only be found by investigating the behavior of $u(\xi)$ in the region downstream of the subshock. We rewrite Equation (15) as 2-D autonomous system:

$$\mathrm{d}u/\mathrm{d}\xi = Q_g/(\eta_g - 2u)\,, \tag{19a}$$

$$\mathrm{d}Q_g/\mathrm{d}\xi = D_{RC} - [\gamma\eta_g - (\gamma + 1)u]Q_g/(\eta_g - 2u)\,. \tag{19b}$$

It can be shown by critical-point analysis that condition (12) is the decisive criterion for the above question. If the solution $u = u^*$ satisfies the equilibrium equation $\rho Q(T) - \rho_1 Q(T_1) = 0$, i.e., $D_{RC} = 0$, then the point $(u, Q_g) = (u^*, 0)$ is a critical point of the system (19). When the condition (12) is not satisfied, $(u^*, 0)$ is an unstable node or an unstable spiral point – in the phase plane of (u, Q_g), all trajectories near the point $(u^*, 0)$ move away from it as $\xi \to -\infty$. The physical interpretation is that radiative cooling drives the system away from the equilibrium. By contrast, $(u^*, 0)$ becomes a saddle point when α satisfies condition (12). That is, trajectories near this point approach it in a specific direction, and move away from it in the other direction. Only one trajectory reaches this point as $\xi \to -\infty$ (see Bender and Orszag, 1978), and this special trajectory corresponds to the expected physical solution. In other words, the system approaches the appropriate equilibrium in the downstream region when $\alpha > (\eta_g - u^*)/(\eta_g - 2u^*)$.

For example, when $\alpha = 2$, the autonomous system (19) has thre critical points, namely, $(u, Q_g) = (1, 0)$, $(u_2, 0)$, and $(u_+, 0)$. Point $(u_2, 0)$ corresponds to the physical solution, and this point is a saddle point near which trajectories approach it in the direction $\mathrm{d}Q_g/\mathrm{d}u = A_{g+}$ and move away from it in the direction $\mathrm{d}Q_g/\mathrm{d}u = A_{g-}$, where

$$A_{g\pm} = \frac{1}{2}\left\{(\gamma + 1)u_2 - \gamma\eta_g \pm \right.$$
$$\left. \pm \sqrt{[\gamma\eta_g - (\gamma + 1)u_2]^2 + 4(\gamma - 1)R_L \frac{u_c}{u_2} \frac{(\eta_g - 2u_2)(\eta_g - 3u_2)}{T_2}}\right\}. \tag{20}$$

Figure 4 diagrams the saddle point behavior of the solution of the system (19) near the point $(u_2, 0)$. The figure shows that $(u_2, 0)$ can be reached only through the trajectory $(\mathrm{d}Q_g/\mathrm{d}u = A_{g+})$ as $\xi \to -\infty$.

What if $\alpha < (\eta_g - u^*)/(\eta_g - 2u^*)$ and $u_d = u^*$? This special value of u_d corresponds to the solution where equilibrium is reached immediately at the downstream edge of the subshock. For this solution there is no cooling region at all, but the solution is still an unstable one because any tiny deviation from it would immediately drive the system away from equilibrium.

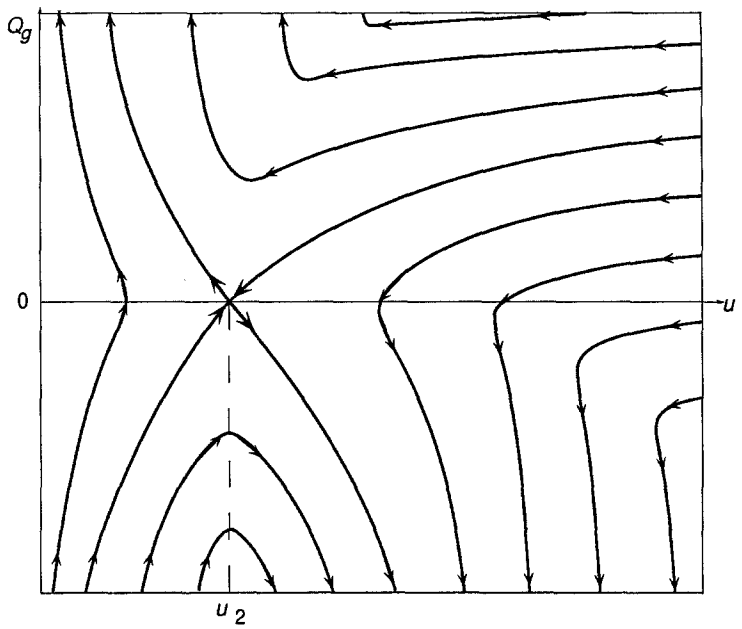

Fig. 4. Schematic plot for solution of system (19) near $(u_2, 0)$ – saddle point behavior ($\alpha = 2$). One, and only one, trajectory would reach $(u_2, 0)$ in the direction $(dQ_g/du)|_2 = A_{g+}$, as $\xi \to -\infty$.

Accordingly, we conclude that the downstream equilibrium can only be reached at a temperature lower than T_c. In other words, the downstream fluid must cool down from its high temperature above T_c to a low temperature below T_c, if it is to reach an equilibrium. The lack of steady-state solutions for $T_d > T_c$ reflects the fact that a plasma on the high-temperature side of the maximum of $Q(T)$ is thermally unstable (Cox and Tucker, 1969).

The velocity u can be obtained by solving Equation (15) numerically. However, an important point has to be taken into consideration in doing the numerical calculation. As mentioned previously, the introduction of radiative cooling changes the jump conditions radically. When radiative cooling is negligible, X, the density jump for total shock, is completely determined by the upstream parameters. However, when radiative cooling is not negligible, X depends not only on the upstream parameters, but also on the shock solution (see above expressions of Δ_g and I_g). That is, we need to know X before solving Equation (15), whereas X depends on the solution of Equation (15). A similar situation also occurs when the radiative MHD equations are solved numerically. We use an iterative method to deal with this problem, and this method is discussed further in the following section and Appendix B.

Figure 5 shows the numerical solution of Equation (15) for $\alpha = 2$. Also shown is the shock solution when radiation is absent. The principal effect of the radiation is to decrease the temperature and flow speed in the downstream cooling region.

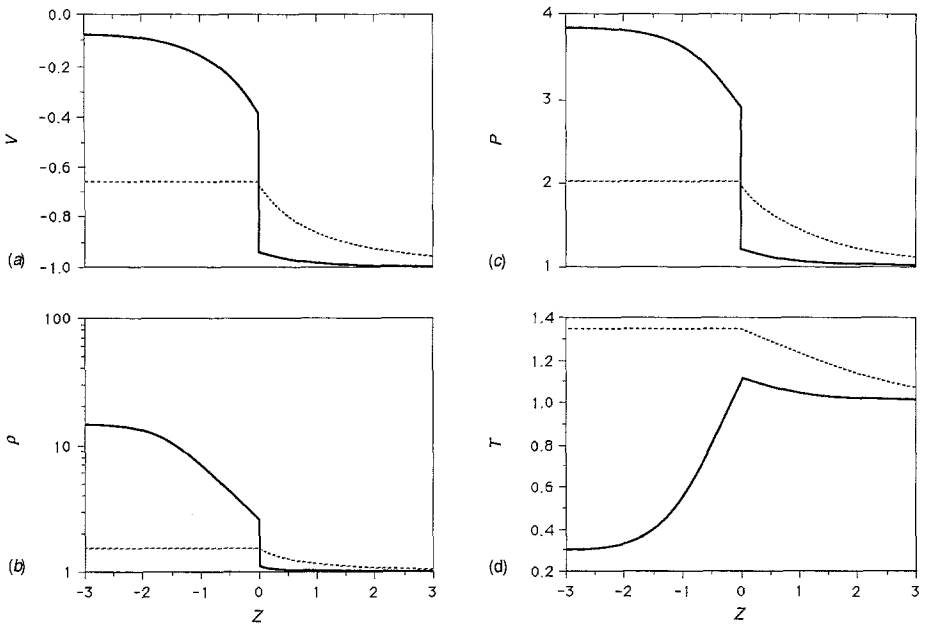

Fig. 5. Numerical solution of radiative gasdynamic shock. From (a) to (d) we plot respectively the variations of the velocity, the density, the pressure, and the temperature in the total shock transition region. The units of T, P, ρ, and V are T_1, P_1, ρ_1, and V_0, respectively, and the upstream conditions are $M_1 = 1.35$, $R_L = 1$, and $u_c = 0.1$. Solutions with no radiation ($R_L = 0$) are also plotted in dashed curves for comparison.

4. Slow-Mode Shocks

In this section we determine the shock structure of MHD slow-mode shocks in the switch-off shock limit. This limit means that there is no tangential magnetic field in the region downstream of the subshock, so for this region the solution is similar to the gas dynamic solution. However, as we will see, in the foreshock region upstream of the subshock it is considerably different. Physically, the most significant difference between the gas dynamic shock and the slow shock is that the gas dynamic shock converts the kinetic energy of the flow into heat, while the slow shock converts magnetic energy into both heat and kinetic energy. As before, the jump conditions at the subshock serve as IBC and the starting point for numerical integration of the shock structure equations. Because these MHD jump relations are much more complicated than the gas dynamic ones, we discuss the MHD jump relations separately before considering the integration of the shock structure equations.

In analyzing shock structure it is very helpful to know what conditions must be given in order to define a unique shock transition. It is well known that for ordinary gas dynamic shocks that, one parameter, such as the upstream Mach number, is enough. By comparison, three parameters are needed for ordinary MHD shocks. For example, the upstream plasma β, the Alfvén Mach number, and the field direction are sufficient. When radiation is taken into consideration, an extra parameter has to be introduced to describe the effect of the radiation. In this paper, R_L – the ratio of the thermal scale

length L_κ to characteristic length of radiative cooling L_R, where $L_\kappa = \gamma\kappa/(\rho_1 c_p V_0)$, $L_R = u_c V_0^3/H_c$, is chosen as the parameter. Since L_κ is also the scale length of the total shock transition, R_L gives a measure of the strength of the radiative cooling.

4.1. Thermal conduction alone

With no radiative cooling, Equations (1) can be integrated across the total shock transition layer (see Figure 2) and rearranged to read

$$\frac{X\beta_1}{\theta_1} + \frac{\gamma - 1}{\gamma}(X + 1) - 2\cos^2\varphi_1 + \left(X - \frac{\gamma - 1}{\gamma}\theta_1\right)\frac{X\theta_1 + \theta_1 - 2X}{(X - \theta_1)^2}\sin^2\varphi_1 = 0\,, \tag{21a}$$

$$Y = 1 + \beta_1^{-1}\{\sin^2\varphi_1 + 2\theta_1\cos^2\varphi_1(1 - 1/X) - [\sin\varphi_1 X(1 - \theta_1)/(X - \theta_1)]^2\}\,, \tag{21b}$$

where X and Y are defined as

$$X = \rho_d/\rho_1 = V_{x1}/V_{xd} = V_0/V_{xd}\,, \qquad Y = P_d/P_1$$

and

$$B_{yd}/B_{y1} = X(1 - \theta_1)/(X - \theta_1)\,, \tag{22a}$$

$$V_{yd} = V_{y1} + V_0\,\mathrm{tg}\,\varphi_1(X - 1)/(X - \theta_1)\,, \tag{22b}$$

$$B_x = B_{x1}\,, \tag{22c}$$

$$\theta_1 = V_0^2/C_{Ax1}^2 \leq 1\,, \tag{22d}$$

$$C_{Ax1}^2 = C_{A1}^2\cos^2\varphi_1 = B_{x1}^2/(\mu\rho_1)\,, \tag{22e}$$

$$\beta_1 = 2\mu P_1/B_1^2\,, \tag{22f}$$

$$\cos\varphi_1 = B_{x1}/B_1\,. \tag{22g}$$

Here β_1, C_{Ax1}, and $\cos\varphi_1$ denote the upstream plasma parameter ($\beta_1 \ll 1$ for solar flares), the Alfvén speed normal to the shock, and the magnetic field direction, respectively.

The above relations are the general jump conditions for MHD slow-mode shocks. The real root (greater than 1) of the cubic equation (21a) gives the density jump X, and all of the other physical parameters can be determined once X is known.

For switch-off shocks (see Figure 6), $B_{yd} = 0$ (i.e., $\theta_1 = 1$), hence the shock speed is the same as upstream Alfvén speed normal to the shock. Accordingly, we obtain

$$X = \frac{1 + \beta_1 + \cos^2\varphi_1 + \sqrt{(\beta_1 + \sin^2\iota\phi_1)^2 + 4\cos^2\varphi_1(1 - \beta_1\gamma)/\gamma^2}}{2[\beta_1 + (\gamma - 1)/\gamma]}\,, \tag{23a}$$

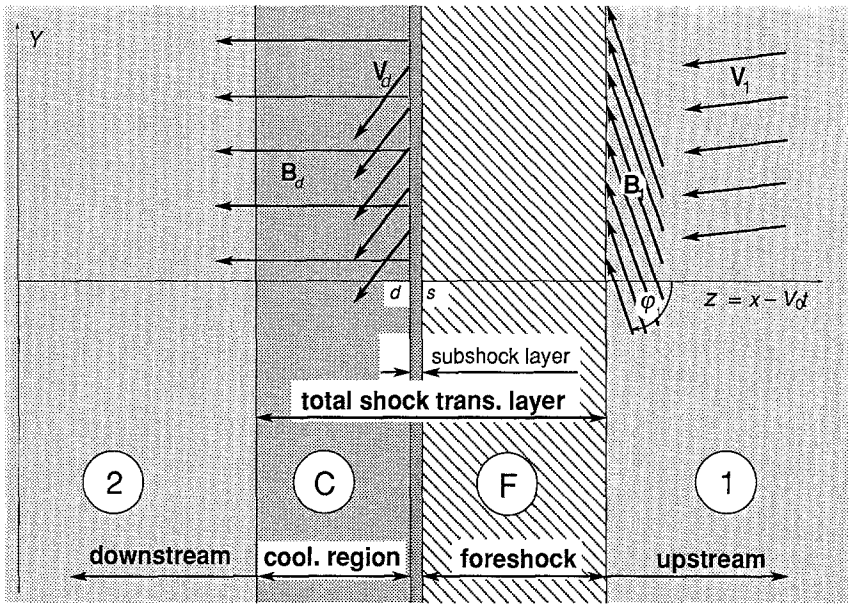

Fig. 6. Schematic geometry of MHD slow-mode switch-off shock.

$$Y = 1 + \beta_1^{-1}(1 + \cos^2\varphi_1 - 2\cos^2\varphi_1/X)\,, \tag{23b}$$

$$V_{yd} = V_{y1} + V_0 B_{y1}/B_{x1}\,. \tag{23c}$$

As mentioned in Section 2, Coroniti's condition has to be satisfied in order for isothermal subshocks to occur, i.e., $V_{xd} < \tilde{C}_{sLd}$, where $\tilde{C}_{sLd}$ is given by the smaller value of Equation (2b).

For switch-off shocks, $\varphi_d = 0$, hence, $C_{Ad}^2 = C_{Axd}^2 = C_{Ax1}^2/X$. From

$$\tilde{C}_{sd}^2 = P_d/\rho_d = C_{Ad}^2\beta_d/2 = YC_{A1}^2\beta_1/2X\,,$$

we find that

$$\beta_d = Y\beta_1 C_{Ax1}^2/C_{Ax1}^2 \approx C_{A1}^2/C_{Ax1}^2 \gg 1\,, \tag{24}$$

since $B_{y1}^2 \gg B_{x1}^2$, i.e., $\tilde{C}_{sd}^2 \gg C_{Ad}^2$.

Therefore, $\tilde{C}_{sLd}^2 = C_{Ad}^2$, and the formation of the isothermal subshock in a slow-mode switch-off shock is ensured because, for $X > 1$,

$$C_{Ax1}/X = V_0/X = V_{xd} < \tilde{C}_{sLd} = C_{Ad} = C_{Ax1}/\sqrt{X}\,. \tag{25}$$

Jump conditions for the isothermal subshock can be derived by integrating Equations (1) across the subshock (from d to s) and using the isothermal condition $T_s = T_d$ to replace the energy equation (1g). Then combining the results with Equations (22) and $v = 0$, $\eta = 0$, we obtain

$$2\theta_1\cos^2\varphi_1(X_s + 1 - X) - X\beta_1 - \\ - X\sin^2\varphi_1\left[1 - \left(\frac{X - X\theta_1}{X - X_s\theta_1}\right)^2\frac{X^2 - X_s\theta_1^2}{(X - \theta_1)^2}\right] = 0\,, \tag{26a}$$

$$B_{ys} = B_{y1} X(1 - \theta_1)/(X - X_s \theta_1)\,, \tag{26b}$$

$$V_{ys} = V_{y1} + V_0 \operatorname{tg} \varphi_1 (X - X_s)/(X - X_s \theta_1)\,. \tag{26c}$$

When $\theta_1 = 1$ (switch-off shock), two possible solutions can be drawn directly from Equation (26b):

(a) $B_{ys} = 0$;

(b) $X = X_s$.

The solution $B_{ys} = 0$ is an impossible result for real shocks, and therefore, for switch-off shocks, the isothermal subshock jump condition is $X_s = X$. The foreshock may then be thought of as a 'tangential shock' because only the tangential components of velocity and magnetic field are changed, while the normal components of velocity and magnetic field remain unchanged.

The jump of the fluid variables are:

$$V_{xs} = V_0\,, \tag{27a}$$

$$\rho_s = \rho_1\,, \tag{27b}$$

$$P_s = P_1 Y/X = P_1 [1 + \beta_1^{-1}(1 + \cos^2 \varphi_1 - 2 \cos^2 \varphi_1 / X)]/X\,, \tag{27c}$$

$$B_{ys}^2 = B_{y1}^2 (X - 1)\,[X + (X\beta_1 - 2 \cos^2 \varphi_1)/\sin^2 \varphi_1\,]/X^2\,, \tag{27d}$$

$$V_{ys} = V_{y1} + V_0 (B_{y1} - B_{ys})/B_{x1}\,. \tag{27e}$$

Table I shows the jump conditions for some typical solar flare loops.

TABLE I

Shock and subshock jump conditions
($T_1 = 2 \times 10^4$ K, $B_1 = 100$ G, $n_1 = 5 \times 10^{10}$ cm^{-3})

Region	M_{1A}	V_x/V_{x1}	V_y/V_{y1}	B_u/B_{u1}	ρ/ρ_1	T/T_1	P/P_1	β
1	0.1	1.00	1.00	1.00	1.00	1.00	1.00	3.47×10^{-4}
	0.01	1.00	1.00	1.00	1.00	1.00	1.00	3.47×10^{-4}
s	0.1	1.00	23.76	0.772	1.00	1.15×10^3	1.15×10^3	0.665
	0.01	1.00	2.26×10^3	0.775	1.00	1.15×10^3	2.89×10^3	0.667
d	0.1	0.399	1.01×10^2	0	2.51	1.15×10^3	2.89×10^3	1.00×10^2
	0.01	0.400	1.00×10^4	0	2.50	1.15×10^3	2.88×10^3	1.00×10^4

$B_{x1}/B_1 = V_0/C_{A1} = V_{y1}/V_0 = M_{1A}$. M_{1A} is the upstream Alfvén Mach number.
$C_{A1} = 9.76 \times 10^2$ km s^{-1} is the upstream Alfvén speed.

The normal fluid velocity and the density are constants in the foreshock region of switch-off shocks. This behavior makes switch-off shocks quite different from gas-dynamic shocks and fast-mode MHD shocks. As Table I shows we expect: $\beta_1 \ll 1$; $\beta_d \gg 1$; $\beta_s \leq 1$; therefore,

$$X \approx (1 + \beta_1 + \gamma^{-2} \cos^2 \varphi_1)/[\beta_1 + (\gamma + 1)/\gamma]\,, \tag{28a}$$

$$Y = \beta_1^{-1}\,, \tag{28b}$$

$$V_{yd} \approx C_{A1}\,, \tag{28c}$$

$$B_{ys} = B_{y1}\sqrt{(X-1)/X}\,. \tag{28d}$$

Equation (28d) implies that of the total energy released by the annihilation of the magnetic field in the shock, about X^{-1} is released in the foreshock region while about $1 - X^{-1}$ is released at the subshock. For typical flare loop conditions $X \approx 3$, therefore above results suggest that about $\frac{2}{3}$ of the magnetic energy will be released at the subshocks, i.e., at the top of the flare loops, while the remaining $\frac{1}{3}$ will be released in the region upstream of the subshocks.

For the near switch-off shocks, the fast wave speed C_{fd} approximately equals C_{sd}, the downstream sound speed, since $B_{yd}/B_{y1} \ll B_{yd}/B_x < 1$ and $\beta_d \gg 1$. Therefore, $V_{yd}^2/C_{fd}^2 \approx 2XY^{-1}\beta_1^{-1}/\gamma \approx 2X/\gamma > 1$, and the downstream flow is supermagnetosonic with respect to the fast-mode wave speed.

When

$$\cos^2\varphi_1 = X(1+\beta_1)/(X+2)\,,$$

$B_{ys} = 0$, $\beta_d = 2$, and hence the subshock is simply a gas dynamic shock for

$$\cos^2\varphi_1 \geq X(1+\beta_1)/(X+2)\,. \tag{29}$$

The subshock vanishes when

$$\beta_d \leq 2/X\,. \tag{30}$$

4.2. Radiation and thermal conduction combined

In the light of the discussion in Section 3, we let $\nu = \eta = 0$ for simplification so that isothermal subshocks reduce to discontinuities. The modification of the jump conditions is discussed first. Next we determine the fluid velocity in the regions upstream and downstream of the subshock. Because the switch-off shock is quite different from the gasynamic shock, the fluid velocity behaves differently than before.

When radiative cooling is taken into account, the jump conditions obtained in Section 4.1 need to be modified correspondingly. Actually, all other relations would remain the same as in Section 4.1 except the expression for X. The equation for X now reads

$$\begin{aligned} &X^2[\beta_1 + (\theta_1 - I_0)(\gamma-1)/\gamma] - X(\beta_1 + 2\theta_1 - \theta_1^2\sin^2\varphi_1) + \\ &\quad + \theta_1\cos^2\varphi_1(\gamma+1)/\gamma + X\theta_1\sin^2\varphi_1(X/\gamma + X - \theta_1)\times \\ &\quad \times [(1-\theta_1)/(X-\theta_1)]^2 = 0\,. \end{aligned} \tag{31}$$

For switch-off shocks,

$$X = \frac{1 + \beta_1 + \cos^2\varphi_1 + \sqrt{(\beta_1 + \sin^2\varphi_1)^2 + 4\cos^2\varphi_1[1 - \beta_1\gamma + (\gamma^2-1)I_0]/\gamma^2}}{2[\beta_1 + (1-I_0)(\gamma-1)/\gamma]}\,, \tag{32}$$

where

$$I_0 = [2M_{1A}^2/(\rho_1 V_0^3)]\left\{(\kappa\, dT/dz)|_d + \int_d^1 \rho[\rho Q(T) - H_c]\, dz\right\} =$$

$$= [2M_{1A}^2/(\gamma - 1)]\left\{(dT/d\xi)|_d + \int_d^1 (\gamma - 1)R_L u_c[\rho_1 Q(T)/H_c - 1]\, d\xi\right\}$$

is the normalized effect of radiative loss as well as the heat flux at the downstream edge of the subshock, and $M_{1A} = V_0/C_{A1}$ is the upstream Alfvén Mach number ($M_{1A} \ll 1$ since $B_{y1} \gg B_{x1}$).

Substituting $B_x = B_{x1}, V_x = V_0, \rho = \rho_1$ into Equations (1), we obtain immediately that in the foreshock

$$V_0 B_y + B_{x1} V_y = V_0 B_{y1} + B_{x1} V_{y1}\,, \tag{33a}$$

$$P + B_y^2/2\mu = P_1 + B_{y1}^2/2\mu\,, \tag{33b}$$

$$d(\kappa\, dT/dz)/dz + \rho_1 V_0 R\,(dT/dz)/(\gamma - 1) - \rho_1[\rho_1 Q(T) - H_c] = 0\,. \tag{33c}$$

Equation (33c) is the critical equation – once it is solved for T, all the other physical parameters are readily obtained. If T is expressed in units of $T_0 = V_0^2/R$, then Equation (33c) is reduced to

$$d^2T/d\xi^2 + dT/d\xi - (\gamma - 1)R_L u_c[\rho_1 Q(T)/H_c - 1] = 0\,, \tag{34}$$

by appropriate normalization (notations follow Equation (15)).

If the radiative loss function $Q(T)$ is fitted with two-component piecewise curve (i.e., $\alpha = 2$ and $\alpha = -\frac{1}{2}$), then by using $\tilde{\gamma}_< T_c^2 = \tilde{\gamma}_> T_c^{-1/2}$, Equation (34) can be written as

$$d^2T/d\xi^2 + dT/d\xi - (\gamma - 1)R_L u_c[(T/T_1)^2 - 1] = 0\,, \qquad T < T_c\,, \tag{35a}$$

$$d^2T/d\xi^2 + dT/d\xi - (\gamma - 1)R_L u_c[T_c^{5/2}/(T_1^2 T^{1/2}) - 1] = 0\,, \; T > T_c\,. \tag{35b}$$

Equations (35) govern the behavior of T in the foreshock region and can be solved numerically.

In the downstream region, the switch-off condition $B_y = 0$ leads to $V_y = V_{yd}$ so that the plasma movement exhibits pure gas dynamic behavior. The equation for $u = V_x/V_0$ is then reduced from Equations (1) by substituting in $B_y = 0$ and $V_y = V_{yd}$ and normalizing. The result is

$$\frac{d^2}{d\xi^2}[u(\eta_0 - u)] + [\gamma\eta_0 - (\gamma + 1)u]\frac{du}{d\xi} - (\gamma - 1)R_L\,\frac{u_c}{u}\left[\frac{\rho_1 Q(T)}{uH_c} - 1\right] = 0\,, \tag{36}$$

where

$$\eta_0 = (P_d + \rho_1 V_0 V_{xd})/(\rho_1 V_0^2) = (P_1 + B_{y1}^2/2\mu + \rho_1 V_0^2)/(\rho_1 V_0^2) =$$
$$= 1 + (\beta_1 + \sin^2\varphi_1)/(2M_{1A}^2) .$$

Equation (36) has the same form as Equation (15) (with Equation (18) substituted in) except η_g is replaced by η_0 ($\eta_0 \gg \eta_g$, since $M_{1A} \ll 1$). Consequently the relevant discussion on Equation (15) can be generalized to include Equation (36). If we define $\eta^* = (P_d + \rho_1 V_0 V_{xd})/\rho_1 V_0^2$, then the condition (12) is generalized as

$$\alpha > \alpha^* = (\eta^* - u^*)/(\eta^* - 2u^*) , \tag{37}$$

where $1 < \alpha^* < \infty$. The quantity η^* describes the normalized total momentum. For gasdynamic shocks, $\eta^* = \eta_g$, while for MHD shocks, $\eta^* = \eta_0$. The quantity u^* is the solution of the equilibrium equation

$$\rho_1 Q(T)/H_c - u = 0 . \tag{38}$$

Again, according to condition (37), when the piecewise α is chosen for the over-all fitting with $Q(T)$, the downstream equilibrium cannot be approached when $T > T_c$. When $T < T_c$, $\alpha = 2$, Equation (38) becomes

$$u(\eta_0 - u)^2 = (T_1 R/V_0^2)^2 .$$

The expected equilibrium velocity is estimated by using $\eta_0 \gg 1$ and $u < 1$ as

$$u^* = u_{-\infty} = u_2 \approx [T_1 R/(\eta_0 V_0^2)]^2 = [\beta_1/(\beta_1 + 2M_{1A}^2 + \sin^2\varphi_1)]^2 \approx \beta_1^2 ,$$

and the equilibrium temperature T_2 is

$$T_2 = u_2(\eta_0 - u_2)V_0^2/R \approx \beta_1 T_1 .$$

The above equilibrium temperature T_2 is estimated for the data in Table I:

$$T_2 \approx \beta_1 T_1 = 3.47 \times 10^{-4} \times 2 \times 10^4 \text{ K} \approx 7 \text{ K} !$$

This unrealisticaly low temperature occurs because we use $\alpha = 2$ to fit with $Q(T)$ for $T < T_c$. However, $\alpha = 2$ is no longer appropriate for $T < 2 \times 10^4$ K since α increases more rapidly in that temperature range. A better fit suggested by Peres *et al.* (1982), that $\alpha = 11.7$ when 4.4×10^3 K $< T < 8 \times 10^3$ K, gives $T_2 = 5.8 \times 10^3$ K. Therefore, a better over-all fit with $Q(T)$ may be obtained by choosing the more precise power law of T, such as

$$\alpha = 10 , \qquad \tilde{\chi} = 3.9 \times 10^{-79} , \qquad T < 2 \times 10^4 \text{ K} ,$$
$$\alpha = 2 , \qquad \tilde{\chi} = 10^{-44} , \qquad 2 \times 10^4 \text{ K} < T < T_c ,$$
$$\alpha = -\tfrac{1}{2} , \qquad \tilde{\chi} = 10^{-31.5} , \qquad T > T_c .$$

Equation (36) can then be combined with above to describe the cooling in the downstream region.

An interesting point worth considering is that the fluid may be heated rather than cooled in the downstream region. It is known that the cooling function $Q(T)$ reaches a maximum at around 10^5 K (i.e., T_c) and a minimum at around 3×10^7 K (i.e., T_{c1}). Hence $\alpha < 0$ for $T_c < T < T_{c1}$, and $\alpha > 0$ for the temperature outside that range. Since values of $\alpha < 0$ never satisfy condition (37), it is impossible for the system to approach the equilibrium when $\alpha < 0$ because of thermal instability. However, when α is sufficiently greater than zero so that condition (37) is satisfied, then in regions where either equilibrium is possible $T > T_{c1}$ or $T < T_c$. The equilibrium in the region where $T < T_{c1}$ implies the heating of the downstream plasma. Since the subshock formation requires $u_2 < \tilde{C}_{sLd}$, an upper limit for the temperature is

$$T_{\max} = T(u = \tilde{C}_{sLd}) \approx T_d X^{1/2} . \tag{39}$$

Therefore, radiative heating can occur for $T_{\max} > 3 \times 10^7$ K, if there is an extra energy source downstream of the subshock.

Since we assume that the subshock is located at $\xi = 0$, the equations which govern the shock structure can be summarized as

$$\mathrm{d}^2T/\mathrm{d}\xi^2 + \mathrm{d}T/\mathrm{d}\xi - (\gamma - 1)R_L u_c[\rho_1 Q(T)/H_c - 1] = 0 , \quad \xi > 0 , \tag{40a}$$

$$\frac{\mathrm{d}^2}{\mathrm{d}\xi^2}[u(\eta_0 - u)] + [\gamma\eta_0 - (\gamma + 1)u]\frac{\mathrm{d}u}{\mathrm{d}\xi} - (\gamma - 1)R_L \frac{u_c}{u}\left[\frac{\rho_1 Q(T)}{uH_c} - 1\right] = 0 , \quad \xi < 0 . \tag{40b}$$

In order to solve Equations (40), we have first to calculate the necessary IBC because $u(\xi)$ and $T(\xi)$ cannot be integrated numerically from $-\infty$ or ∞. The numerical calculation has to start from the subshock, i.e., $\xi = 0$.

Let $\xi = 0^+$ and $\xi = 0^-$ denote the upstream and the downstream edges of isothermal subshock. The following equations are obtained by integrating Equations (40a) and (40b) from $\xi = 0^+$ to ∞, and $\xi = -\infty$, respectively:

$$Q_{ms} + R_{cu} = [X\beta_1 - (1 + \cos^2\varphi_1 - 2\cos^2\varphi_1/X + \beta_1)]/(2XM_{1A}^2) , \tag{41a}$$

$$Q_{md} - R_{cd} = (u_2 - 1/X)[\gamma\eta_0 - (u_2 + 1/X)(\gamma + 1)/2] . \tag{41b}$$

Equation (32) can be rewritten as

$$Q_{md} + R_{cu} = [\beta_1\gamma + \gamma - 1 - \gamma(\beta_1 + 1 + \cos^2\varphi_1)/X + (\gamma + 1)\cos^2\varphi_1/X^2]/(2M_{1A}^2) , \tag{41c}$$

where $Q_m = \mathrm{d}T/\mathrm{d}\xi$ is the normalized heat flux ($\kappa\nabla T$) with T expressed in units of V_0^2/R, R_{cu} and R_{cd} are the energy losses due to radiation in the foreshock and cooling regions, respectively:

$$R_{cu} = \int_{0^+}^{\infty} (\gamma - 1)R_L u_c[\rho_1 Q(T)/H_c - 1]\,\mathrm{d}\xi ,$$

$$R_{cd} = \int_{-\infty}^{0^-} (\gamma - 1) R_L \frac{u_c}{u} [\rho_1 Q(T)/(uH_c) - 1] \, d\xi .$$

The three equations above are not enough to determine the five unknowns X, R_{cu}, R_{cd}, Q_{ms}, and Q_{md}, which are needed to solve $T(\xi)$ in the upstream region and $u(\xi)$ in the downstream region. Thus to obtain additional constraints we rewrite Equations (40) as

$$dQ_m/du + \gamma\eta_0 - (\gamma + 1)u - (\gamma - 1)R_L u_c[(\eta_0 - u)^2/T_1^2 - 1/u] \times$$
$$\times (\eta_0 - 2u)/Q_m = 0 , \qquad u_2 < u < u_d ,$$
$$dQ_m/dT + 1 - (\gamma - 1)R_L u_c[(T/T_1)^2 - 1]/Q_n = 0 , \qquad T_1 < T < T_d ,$$

where the piecewise α with two components has been used to fit $Q(T)$. Two initial conditions can then be drawn by taking the limit $u \to u_2$ and $T \to T_1$ in the two equations above, namely,

$$\left.\frac{dQ_m}{du}\right|_2 = \frac{(\gamma + 1)u_2 - \gamma\eta_0}{2} + \sqrt{\frac{[\gamma\eta_0 - (\gamma + 1)u_2]^2}{4} + (\gamma - 1)R_L u_c \frac{(\eta_0 - 2u_2)(\eta_0 - 3u_2)}{u_2 T_2}} , \tag{41d}$$

$$(dQ_m/dT)|_1 = -[1 + \sqrt{1 + 8(\gamma - 1)R_L u_c/T_1}]/2 . \tag{41e}$$

To determine Q_{md} and Q_{ms}, Equation (40a) is integrated from $u = u_2$, $Q_m = 0$ to $u = u_d$, $Q_m = Q_{md}$, while Equation (40b) is integrated from $T = T_1$, $Q_m = 0$ to $T = T_s$, $Q_m = Q_{ms}$. These coupled equations are solved iteratively until the values converge. Once Q_{md} and Q_{ms} are known, X, R_{cu}, and R_{cd} can be obtained from Equations (41). In turn $u(\xi)$ and $T(\xi)$ can be calculated by integrating Equations (40a) and (40b) from the subshock towards the downstream and the upstream regions.

In Figure 7, we plot an example of the structure of a radiative slow shock from the far upstream region through to the far downstream region. When compared with the shock solution with no radiation ($R_L = 0$, shown by the dashed curve), the figure shows that the radiation in the downstream region is much stronger than it is in the upstream region. Apparently this occurs because downstream of the subshock the density is much higher. Due to the switch-off limit, the radiation has almost no effect on the pressure and the tangential components of the velocity and the field, though it does substantially change the temperature, the density, and the normal velocity in the downstream region.

Figure 8 shows the variation of the magnetic, kinetic and internal energy through the shock and the downstream cooling region. Also shown are the plasma parameter, the heat flux, and the fast mode Mach number. The effect of the radiation is to greatly increase the Mach number which is about 1.7 (for $\gamma = \frac{5}{3}$) in the absence of the radiation.

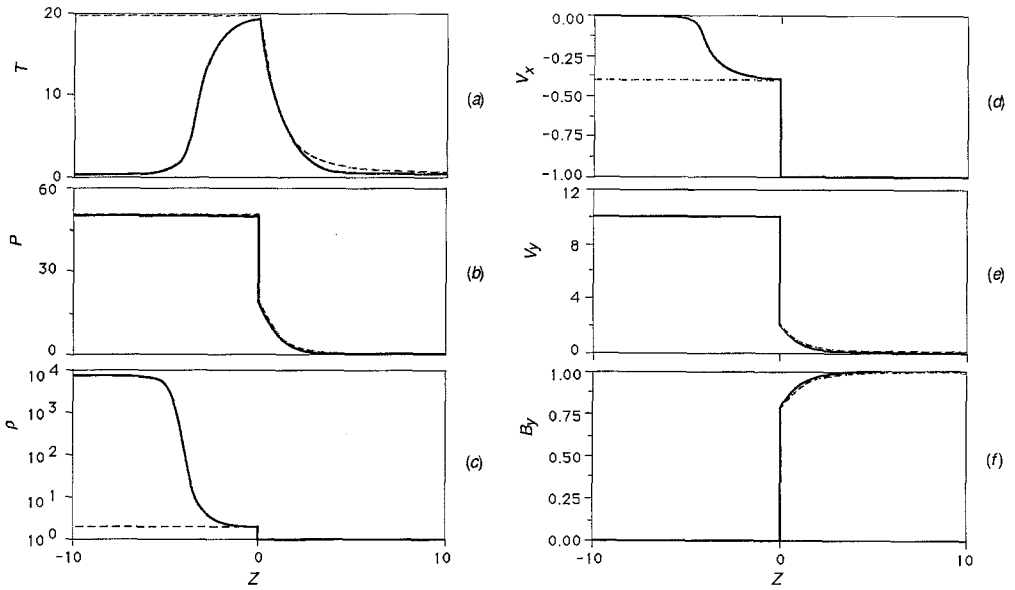

Fig. 7. A numerical solution of an MHD switch-off shock. From (a) to (f), T, P, ρ, V_x, V_y, B_y are in the units of V_0^2/R, $\rho_1 V_0^2$, ρ_1, V_0, V_0, and B_{y1}, respectively. The Alfvén Mach number $M_{1A} = \cos\varphi_1 = 0.1$, $\beta_1 = 3.47 \times 10^{-4}$, and $R_L = 1$, where a 3-component α fit has been used for $Q(T)$. Solutions with no radiation ($R_L = 0$) are shown by the dashed curves.

To show how the shock structure varies with the strength of the radiative loss, we plot the temperature jump across the total shock transition. As shown in Figure 9, the temperature jump is nearly constant as R_L, the ratio of radiative to conduction scale lengths, increases. However, at R_L near 1, the temperature jump suddenly decreases. This sudden decrease is due to the fact that for $R_L > 1$, the radiative scale length becomes smaller than the thermal conduction scale length. When this happens, the radiation loss isgreater than the amgnetic energy available in the total shock transition, and the shock can be maintained only by drawing more energy from the inflow plasma. This is done by greatly changing the structure of the shock. Thus the sudden transfer of the curve from nearly horizontal to steep falling at $R_L = 1$ suggests that the shock is nearly getting destroyed when the characteristic length of radiative cooling is less than the thermal scale length.

5. Summary

In the presence of strong thermal conduction an MHD slow shock dissociates into foreshock, which is dominated by heat-flux transport, and an isothermal subshock, which is dominated by viscous dissipation. The addition of radiation creates a third region immediately downstream of the subshock, and in this region radiative cooling dominates. For coronal conditions typical of flare loops, the radiation in the downstream region is much stronger than it is in the foreshock. Because of the thermal

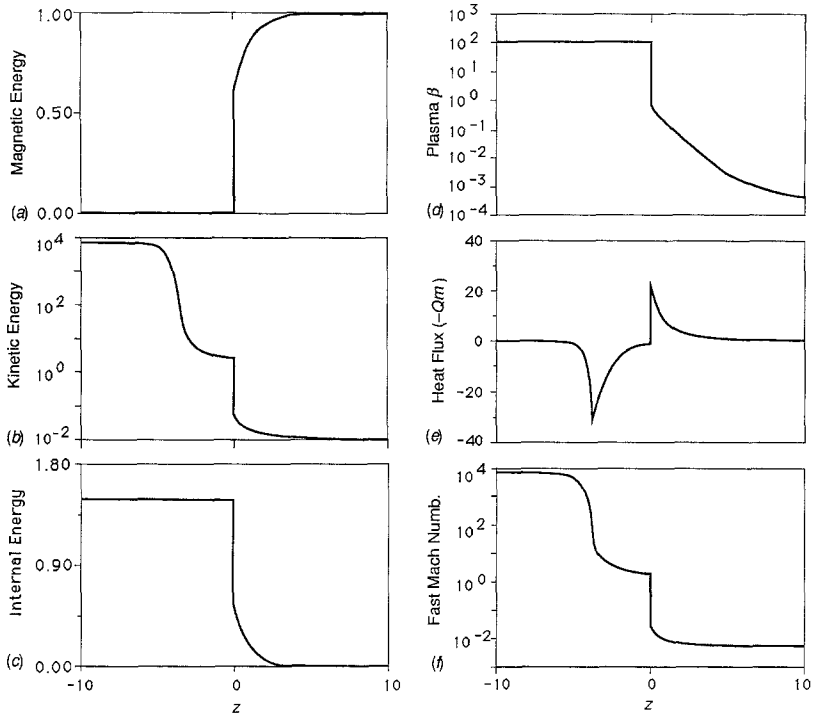

Fig. 8. Various physical quantities across the total transition layer: (a) magnetic energy $B^2/2\mu$; (b) kinetic energy $\rho(V_x^2 + V_y^2)/2$; (c) internal energy $P/(\gamma - 1)$: (d) plasma β; (e) heat flux $-Q_m$; (f) fast Mach number V^2/C_f^2, where the unit of the heat flux is V_0^2/RL_κ, and all the energies are normalized by the upstream total energy. The upstream parameters are the same as for Figure 7.

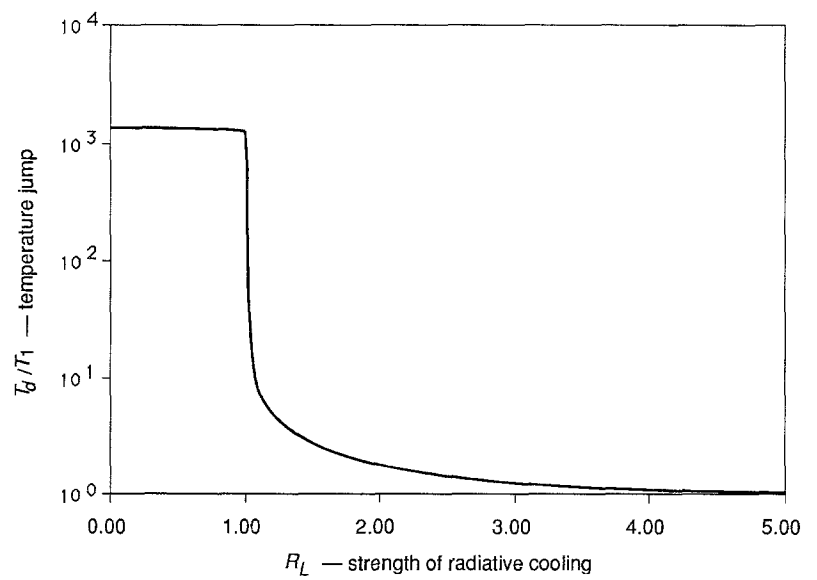

Fig. 9. The temperature jump across the total shock T_1 vs R_L, the strength of the radiative cooling. M_{1A}, $\sin\varphi_1$, and β_1 are the same as in Figures 7 and 8.

conduction, the downstream cooling region is strongly coupled to the foreshock, and the determination of the shock structure requires simultaneous solution of the equations governing all three regions.

For typical flare conditions, we find that the pressure jump across the total shock transition is nearly equal to β_1^{-1}, where β_1 is the upstream plasma β. The downstream tangential velocity is about the same as the upstream Alfvén speed, supermagnetosonic with respect to the fast-mode wave speed. The tangential magnetic field (normalized by upstream tangential field) at upstream edge of the subshock is close to $(1 - X^{-1})^{1/2}$, where X is the density jump across the total shock. This indicates that of the total energy released by the annihilation of magnetic field, about $\frac{1}{3}$ ($\sim X^{-1}$) is released in the foreshock region while remaining $\frac{2}{3}$ ($\sim 1 - X^{-1}$) is released at the subshock. Since the thickness of total shock transition is of the order of the scale-size of flare loops, this result suggests that the magnetic energy release occurs not only at the top of the flare loop (where the x-line is), but also throughout the entire length of the loop.

In a previous order-of-magnitude analysis of flare loops, Forbes, Malherbe, and Priest (1989) assumed that almost all of the energy release occurs in the subshock, and that the thermal energy conducted into the foreshock region was on the order of the radiative loss there. However, our analysis of the structure of slow shocks implies that substantial (up to $\frac{1}{3}$) of the energy release occurs in the foreshock region and that it is the radiative loss in the downstream cooling region rather than the foreshock region, which is of the same order as the energy conducted into the foreshock. Therefore, the balance between the radiative cooling and thermal heating is never reached in the foreshock. Instead, it might occur in the downstream of the subshock, although we do not know whether this will really be the case in the flare loops, since a full two-dimensional solution will be necessary to determine the correct behavior.

A criterion for equilibrium in the far downstream, i.e., inequality (37), has been derived by critical-point analysis. It shows that no stable, steady-state solutions exist for radiative slow shocks unless the temperature in the downstream region of the subshock falls below 10^5 K.

Appendix A. About Criterion (12)

We present here the derivation of criterion (12) by using the critical-point analysis (see Bender and Orszag, 1978, for further discussion). We start by normalizing Equation (7) into a 1-D autonomous system:

$$[\gamma \eta_g - (\gamma + 1)u]\, \mathrm{d}u/\mathrm{d}\xi = u_c R_L (\gamma - 1)\, [Q(T)/Q(T_1) - u]/u^2 . \tag{A-1}$$

If $u = u^*$ satisfies

$$Q(T) - uQ(T_1) = 0 , \tag{A-2}$$

and the appropriate physical conditions are applied, then $u = u^*$ represents the solution to the downstream equilibrium. The stability of this solution can be analyzed by examining the behavior of (A-1) near critical point $u = u^*$ through critical-point analysis.

The quantity $Q(T)$ can be written as

$$Q(T) = \tilde{\gamma}(V_0^2/R)^{\alpha} u^{\alpha}(\eta_g - u)^{\alpha} = C_{\chi} u^{\alpha}(\eta_g - u)^{\alpha},$$

so that Equation (A-2) gives

$$u^{*\alpha-1}(\eta_g - u^*)^{\alpha} = Q(T_1)/C_{\chi}. \tag{A-3}$$

Substituting $u = u^* + \varepsilon$ into Equation (A-1) and linearizing it by letting $\varepsilon \to 0$, we get

$$[\gamma\eta_g - (\gamma+1)u^*]\frac{d\varepsilon}{d\xi} \approx u_c R_L \frac{\gamma-1}{u^*}\left(\frac{\alpha-1}{u^*} - \frac{\alpha}{\eta_g - u^*}\right)\varepsilon. \tag{A-4}$$

Therefore, when $\varepsilon \approx 0$,

$$\varepsilon \to \exp\left\{\frac{u_c(\gamma-1)R_L}{u^*[\eta_g - (\gamma+1)u^*]}\left(\frac{\alpha-1}{u^*} - \frac{\alpha}{\eta_g - u^*}\right)\xi\right\}. \tag{A-5}$$

The condition $u \to u^*$ as $\xi \to -\infty$ (in the downstream region) requires

$$(\alpha-1)/u^* - \alpha/(\eta_g - u^*) > 0,$$

i.e.,

$$\alpha(\eta_g - u^*) - \alpha u^* > \eta_g - u^*,$$

which is equivalent to criterion (12), that is

$$\alpha > (\eta_g - u^*)/(\eta_g - 2u^*).$$

Appendix B. Some Notes on Numerical Calculation

The critical-point analysis indicates that the solutions satisfying the upstream and the downstream equilibrium conditions correspond to two saddle points. The saddle point behavior makes it difficult to solve Equations (40) numerically because of the bad convergence properties. Near the saddle point any tiny numerical error drives the numerical result far away from the exact solution. This situation can only be avoided by starting the calculation from the saddle point itself. Therefore, the calculation is carried out in two steps. First, starting the integration from $u = u_2$ and $T = T_1$, we calculate $Q_m(u)$ and $Q_m(T)$ by iterating to obtain the necessary inner boundary conditions. Then, $u(\xi)$ and $T(\xi)$ are calculated subsequently, by starting from the subshock.

We transform Equations (40) into the following new form for a piecewise α with two components:

For $\xi > 0$,

$$y_1' = 1,$$

$$y_2' = \begin{cases} -1 + (\gamma-1)u_c[y_1^2/y_{10}^2 - 1]R_L/y_2, & y_1 < y_{1c}, \\ -1 + (\gamma-1)u_c(y_{1c}^{5/2} y_{10}^{-2} y_1^{-1/2} - 1)R_L/y_2, & y_1 > y_{1c}, \end{cases} \tag{B-1}$$

where

$$y_1 = T, \qquad y_2 = Q_m = \mathrm{d}T/\mathrm{d}\xi,$$

with initial conditions

$$y_1(0) = y_{10} = T_1, \qquad y_1'(0) = 1,$$

$$y_2(0) = Q_{m1}, \qquad y_2'(0) = (\mathrm{d}Q_m/\mathrm{d}T)|_1,$$

where $y_2'(0)$ is given by Equation (41b), y_{1c} corresponds to T_c.

For $\xi < 0$,

$$y_1' = 1,$$

$$y_2' = \begin{cases} -\gamma\eta_0 + (\gamma+1)y_1 + f\left[\dfrac{y_1(\eta_0 - y_1)^2}{y_{10}^2(\eta_0 - y_{10})^2} - 1\right], & y_1 < y_{1c}, \\ -\gamma\eta_0 + (\gamma+1)y_1 + f\left\{\dfrac{T_c^2}{T_1^2}\left[\dfrac{y_{1c}(\eta_0 - y_{1c})}{y_1^3(\eta_0 - y_1)}\right]^{1/2} - 1\right\}, & y_1 > y_{1c}, \end{cases} \tag{B-2}$$

where

$$y_1 = u,$$

$$y_2 = Q_m = (\eta_0 - 2y_1)\,\mathrm{d}y_1/\mathrm{d}\xi,$$

$$f = (\gamma - 1)R_L u_c(\eta_0/y_1 - 2)/y_2,$$

with initial conditions

$$y_1(0) = y_{10} = u_2, \qquad y_1'(0) = 1,$$

$$y_2(0) = Q_{m2}, \qquad y_2'(0) = (\mathrm{d}Q_m/\mathrm{d}u)|_2.$$

Picking $T_d^{(0)} > T_1$ as the starting point, the iteration runs as follows: first, integrate Equations (B-1) from T_1 to $T_d^{(0)}$ to get $R_{cu}^{(1)}$, the first estimate of R_{cu}. Next, integrate Equations (B-2) from u_2 to $u_d^{(0)}$, where $u_d^{(0)}$ is calculated from the equation of state $T_d = u_d(\eta_0 - u_d)$ to get $Q_{md}^{(1)}$, the first estimate of Q_{md}. Then $u_d^{(1)}$, the first estimate of $u_d = X^{-1}$, can be obtained by substituting $R_{cu}^{(1)}$ and $Q_{md}^{(1)}$ to Equation (41c) and solving it. Finally, $T_d^{(1)}$ can be solved from this equation. Accordingly, $T_d^{(2)} \ldots T_d^{(n)}$ are calculated by iterations until $|T_d^{(n)} - T_d^{(n+1)}| < \varepsilon$ or $n > N$, where ε and N are the predetermined error and iteration time, respectively.

In our computation we have done numerical integration by using a standard fourth-order Runge–Kutta algorithm.

References

Bel Ni, and L.-Micoulaut, C. J.: 1973, *J. Plasma Phys.* **10**, 301.

Bender, C. M. and Orszag, S. A.: 1978, *Advanced Mathematical Methods for Scientists and Engineers*, Ch. 9, McGraw-Hill Book Co., New York.

Cargill, P. J. and Priest, E. R.: 1982, *Solar Phys.* **76**, 357.

Chevalier, R. A.: 1974, *Astrophys. J.* **188**, 501.
Chevalier, R. A. and Theys, J. C.: 1975, *Astrophys. J.* **195**, 53.
Coroniti, F. V.: 1970, *J. Plasma Phys.* **4**, 265.
Cox, D. P.: 1972a, *Astrophys. J.* **178**, 143.
Cox, D. P.: 1972b, *Astrophys. J.* **178**, 159.
Cox, D. P. and Tucker, W. H.: 1969, *Astrophys. J.* **157**, 1157.
Edmiston, J. P. and Kennel, C. F.: 1986, *J. Geophys. Res.* **91**, 1361.
Feldman, W. C., Schwartz, S. J., Bame, S. J. *et al.*: 1984, *Geophys. Res. Letters* **11**, 599.
Feldman, W. C., Baker, D. N., Bame, S. J., Birn, J., Gosling, J. T., Hones, E. W., Jr., Schwartz, S. J., and Zwickl, R. D.: 1985, *J. Geophys. Res.* **90**, 233.
Feldman, W. C., Tokar, R. L., Birn, J., Hones, E. W., Jr., Bame, S. J., and Russell, C. T.: 1987, *J. Geophys. Res.* **92**, 531.
Forbes, T. G.: 1986, *Astrophys. J.* **305**, 553.
Forbes, T. G. and Malherbe, J. M.: 1986a, *Astrophys. J.* **302**, L67.
Forbes, T. G. and Malherbe, J. M.: 1986b, in D. F. Neidig (ed.), *The Lower Atmosphere of Solar Flares*, National Solar Observatories, Sacramento Peak, NM, NSO, p. 443.
Forbes, T. G., Malherbe, J. M., and Priest, E. R.: 1989, *Solar Phys.* **120**, 258.
Giovanelli, R. G.: 1947, *Monthly Notices Roy. Astron. Soc.* **107**, 338.
Hada, T. and Kennel, C. F.: 1985, *J. Geophys. Res.* **90**, 531.
Heinzel, P. and Karlický, M.: 1987, *Solar Phys.* **110**, 343.
Hirayama, T.: 1974, *Solar Phys.* **34**, 323.
Kantrowitz, A. R. and Petschek, H. E.: 1966, in W. B. Kunkel (ed.), *Plasma Physics in Theory and Application*, McGraw-Hill, New York, p. 147.
Kennel, C. F.: 1987, *J. Geophys. Res.* **92**, 13427.
Kennel, C. F.: 1988, *J. Geophys. Res.* **93**, 8545.
Kleczek, J.: 1964, in W. H. Hess (ed.), *AAS–NASA Symposium on the Physics of Solar Flares*, NASA SP-50, p. 77.
Kopp, R. A. and Pneuman, G. W.: 1976, *Solar Phys.* **50**, 85.
Lin, H.-A., Lin, R. P., and Kane, S. R.: 1985, *Solar Phys.* **99**, 263.
Low, B. C. and Wolfson, R.: 1988, *Astrophys. J.* **324**, 574.
Malherbe, J. M., Forbes, T. G., and Priest, E. R.: 1984, *The Hydromagnetics of the Sun*, ESA SP-220, p. 119.
Marshak, R. E.: 1958, *Phys. Fluids* **1**, 24.
Ohki, K.: 1975, *Solar Phys.* **45**, 435.
Parker, E. N.: 1963, *Astrophys. J. Suppl. Ser.* **8**, 177.
Parker, E. N.: 1984, in E. W. Hones, Jr. (ed.), *Magnetic Reconnection in Space and Laboratory Plasmas*, AGU, Washington, D.C., p. 32.
Peres, G., Rosner, R., Serio, S., and Vaiana, G. S.: 1982, *Astrophys. J.* **252**, 791.
Petschek, H. E.: 1964, in W. H. Hess (ed.), *AAS–NASA Symposium on the Physics of Solar Flares*, NASA SP-50, p. 425.
Priest, E. R.: 1982a, *Solar Phys.* **86**, 33.
Priest, E. R.: 1982b, *Solar Magnetohydrodynamics*, Ch. 2, D. Reidel Publ. Co., Dordrecht, Holland.
Priest, E. R.: 1984, in E. W. Hones, Jr. (ed.), *Magnetic Reconnection in Space and Laboratory Plasmas*, AGU, Washington, D. C., p. 63.
Priest, E. R.: 1985, paper presented at Meeting on SOHO and Cluster Missions, Eur. Space Agency, Garmish, Germany.
Priest, E. R. and Forbes, T. G.: 1986, *J. Geophys. Res.* **91**, 5579.
Richter, A. K.: 1988, in V. J. Pizzo, T. E. Holzer, and D. G. Sime (eds.), *Proceedings of the Sixth International Solar Wind Conference*, NCAR Tech. Note 306, Boulder, p. 411.
Rosenau, P. and Frankenthal, S.: 1978, *Phys. Fluids* **21** (4), 559.
Schmieder, B., Forbes, T. G., Malherbe, J. M., and Machado, M. E.: 1987, *Astrophys. J.* **317**, 956.
Sonnerup, B. U. Ö.: 1979, in L. Lanazerotti, C. Kennel, and . N. Parker (eds.), *Solar System Plasma Physics*, Vol. III, Ch. 3, Section 1, 2, North-Holland, Amsterdam.
Sonnerup, B. U. Ö.: 1984, in D. M. Butler and K. Papadopulos (eds.), *Solar Terrestrial Physics: Present and Future*, Ch. 1, NASA Ref. Publ., RP-1120.
Sturrock, P. A.: 1972, in R. Ramaty and R. G. Stone (eds.), *High Energy Phenomena on the Sun*, NASA, p. 3.

Sweet, P. A.: 1958, in B. Lehnert (ed.), *Electromagnetic Phenomena in Cosmical Physics*, Cambridge University Press, London, p. 123.
Swift, D. W.: 1983, *J. Geophys. Res.* **88**, 5685.
Winske, D., Storer, E. K., and Gray, S. P.: 1985, *Geophys. Res. Letters* **12**, 295.
Withbroe, G. L.: 1978, *Astrophys. J.* **225**, 641.
Zirin, H.: 1986, in D. F. Neidig (ed.), *The Lower Atmosphere of Solar Flares*, National Solar Observatories, Sacramento Peak, NM, p. 78.